

Classification: Biological Science - Neuroscience

**Deficits in microRNA-mediated Cxcr4/Cxcl12 signaling in neurodevelopmental deficits
in a 22q11-deletion syndrome mouse model.**

by

Michihiro Toritsuka^{a,b,1}, Sohei Kimoto^{a,b,1}, Kazue Muraki^{a,1},

Melissa A. Landek-Salgado^c, Atsuhiko Yoshida^d, Norio Yamamoto^d, Yasue Horiuchi^e, Hideki Hiyama^{c,e}, Katsunori

Tajinda^{c,e}, Ni Keni^e, Elizabeth Illingworth^f,

Takashi Iwamoto^g, Toshifumi Kishimoto^b, Akira Sawa^c and Kenji Tanigaki^{a,2}

^aResearch Institute, Shiga Medical Center, Shiga, Japan

^bDepartment of Psychiatry, Nara Medical University Faculty of Medicine, Nara, Japan

^cDepartment of Psychiatry and Behavioral Sciences, Johns Hopkins University School of Medicine, Baltimore, MD, USA

^dDepartment of Otolaryngology, Head and Neck Surgery, Graduate School of Medicine, Kyoto University, Kyoto Japan

^ePharmacology Research Labs, Astellas Pharma Inc., Tsukuba, Japan

^fUniversity of Salerno, Fisciano, Italy

^gDepartment of Biomedical Sciences, College of Life and Health Sciences, Chubu University, Aichi, Japan

¹These authors contributed equally to this work

²Correspondence should be addressed to K. T. (tanigaki@res.med.shiga-pref.jp)

Abstract

22q11 deletion syndrome (22q11DS) frequently accompanies psychiatric conditions, some of which are classified as schizophrenia and bipolar disorder in the current diagnostic categorization. However, it remains elusive how the chromosomal microdeletion leads to the mental manifestation at the mechanistic level. Here we show that a 22q11 DS mouse model with deletion of 18 orthologous genes of human 22q11 (*Df1/+* mice) has deficits in migration of cortical interneurons and hippocampal dentate precursor cells. Furthermore, *Df1/+* mice show functional defects in *Cxcr4/Cxcl12* (*Sdf1*) signaling, which reportedly underlie interneuron migration. Notably the defects in interneuron progenitors are rescued by ectopic expression of *Dgcr8*, one of the genes in 22q11 microdeletion. Furthermore, heterozygous knockout mice for *Dgcr8* show similar neurodevelopmental abnormalities as *Df1/+* mice. Thus, *Dgcr8*-mediated regulation of miRNA is likely to underlie *Cxcr4/Cxcl12* signaling and associated neurodevelopmental defects. Finally, we observe that expression of *CXCL12* is decreased in olfactory neurons from sporadic cases with schizophrenia compared with normal controls. Given the increased risk of 22q11DS in schizophrenia that frequently shows interneuron abnormalities, the overall study suggests that *CXCR4/CXCL12* signaling may represent a common downstream mediator in the pathophysiology of schizophrenia and related mental conditions.

Significance Statement

22q11 deletion syndrome (22q11DS) is a chromosome disorder which frequently accompanies psychiatric conditions such as schizophrenia. However, it remains elusive how the chromosomal microdeletion causes the mental manifestation. Here we show that a 22q11DS mouse model has deficits in the development of interneurons and hippocampal dentate gyrus (DG) and that *Dgcr8*, a microprocessor of miRNA, one of the genes in 22q11 underlies these neurodevelopmental abnormalities. *Dgcr8* regulates *Cxcr4/Cxcl12* (*Sdf1*) signaling, which is indispensable for interneuron and DG development. Finally, we observe that decreased expression of *CXCL12* in olfactory neurons from sporadic schizophrenia. Given the increased risk of 22q11DS in schizophrenia, the overall study suggests that *CXCR4/CXCL12* signaling may represent a common downstream mediator in the pathophysiology of schizophrenia.

¥body

Introduction

22q11.2 deletion syndrome (22q11DS) is frequently associated with major mental conditions, such as schizophrenia (SZ) (1). Some reports have indicated that 22q11DS might account for up to 1~2% of subjects diagnosed as SZ (2, 3). All of the genes, except for one, in the human 22q11.2 locus exist on mouse chromosome 16, although the organization is different (4). This has facilitated the generation of mouse models of 22q11DS, which carry different size hemizygous deletions of the 22q11-related region (5-8). These mouse models include *Df1/+* and *LgDel/+* mice: the former has a deletion from *Es2* to *Ufd1l*, whereas the latter has a deletion from *Idd* to *Hira*. A recent study using the *LgDel/+* mouse model showed that the hemizygous deletion of the 22q11-related region led to delayed migration of interneurons, altered distribution of parvalbumin (PV)-positive interneurons (9), and reduced *Cxcr4* expression known to play a role in interneuron migration (10), although it remains to be determined whether *Cxcr4* signaling is impaired or not in this model mice. Given that changes in the PV-positive interneurons occur in the pathology of SZ (11, 12), these reports are intriguing. Nonetheless, the mechanism and clinical evidence that link these phenotypic changes are unclear.

Dgcr8 is one of the genes in the 22q11-related region, and has been proposed to be responsible, at least in part, for psychiatric manifestations (13). *Dgcr8* heterozygous knockout mice show working memory deficits and sensory information-processing deficits (6, 14), which are also seen in SZ patients. However, it remains elusive how the deficit of this specific molecule can underlie these behavior changes.

Here we show that another mouse model of 22q11DS, *Df1/+* mice, which have a shorter deletion of the 22q11-related region, also have abnormal interneuron migration. Using *Df1/+* and *Dgcr8* heterozygous knockout mice, we directly demonstrate that interneuron progenitors show deficits in *Cxcr4/Cxcl12* signaling, and that *Cxcr4*-dependent hippocampus dentate gyrus (DG) development is also affected. Furthermore, the decreased preference of *Df1/+* interneuron progenitors for *Cxcl12* could be rescued by overexpression of *Dgcr8*, suggesting the involvement of *Dgcr8*-regulated miRNA in this deficit. Finally, we provide evidence that *Cxcl12* is downregulated in the olfactory epithelium from SZ patients.

Results

***Dfl*/+ mice show interneuron migration deficits.**

To determine which genes are responsible for interneuron migration deficits we examined *Dfl*/+ mice, which have a shorter deletion compared with *LgDel*/+ mice (**Supplementary Fig. 1A**). Immunohistochemical studies of Lhx6 and Gad67 showed that the distribution of interneurons was altered at E18.5; with a reduced number in the marginal zone (MZ) and an increased number in the deep cortical plate (dCP) [Lhx6, genotype x layer interaction, $F_{4,16}=8.81$, $p=0.0006$ ($n=3$, embryos); Gad67, genotype x layer interaction, $F_{4,16}=5.50$, $p=0.0056$ ($n=3$, embryos) (ANOVA)] (**Fig.1A,B, Supplementary Fig.1B, C**). Furthermore, the number of PV-positive interneurons was decreased in the medial prefrontal cortex of one-month-old *Dfl*/+ mice [control mice; $1.05\pm 0.24\times 10^4$ cells/mm³, *Dfl*/+ mice; $7.74\pm 0.61\times 10^3$ cells/mm³, $p=0.040$ ($n=4-6$) (Student's t test)]. Taken together, these data suggest that at least one of the 18 genes deleted in *Dfl*/+ mice directly underlie interneuron abnormalities.

MGE-derived interneuron progenitors in *Dfl*/+ mice aberrantly respond to Cxcl12.

Previous studies have demonstrated that *Cxcr4*/*Cxcl12* and Neuregulin/*ErbB4* signaling are crucial for cortical interneuron distribution (15-18). Immunohistochemical studies showed that *Cxcr4* expression is decreased in the cortex of E18.5 *Dfl*/+ embryos [genotype, $F_{1,4}=19.50$, $p=0.012$ ($n=3$, embryos) (ANOVA)] (**Fig.1C, D**), which was also reported in *LgDel*/+ mice (10). Furthermore, quantification of the relative fluorescent intensity of *Cxcr4* per cell suggests that each cell expresses less *Cxcr4* (**Fig.1E**). The reduction of *Cxcr4* expression was also confirmed by real-time RT-PCR [$p=0.025$ (Student's t test) ($n=3$, E15.5 embryos)] (**Fig.1F**). In contrast, Neuregulin/*ErbB4* signaling-related genes were not affected in the *Dfl*/+ medial ganglionic eminence (MGE) and cortex (**Supplementary Fig.2**).

Most interneurons are generated from the subpallium including the lateral, medial and caudal ganglionic eminence (LGE, MGE, and CGE) (19, 20). To directly examine the responsiveness of *Dfl*/+ MGE-derived cells to *Cxcl12*, we cocultured E13.5 MGE explants obtained from *Dfl*/+ and control embryos with aggregates of 293T cells expressing *Cxcl12*. This experiment showed the perturbed chemotactic response of *Dfl*/+ MGE-derived

cells to Cxcl12 [genotype, $F_{1,15}=9.37$, $P=0.0079$ (n=8-9, embryos) (ANOVA)] (**Fig.1F-H**).

Hippocampal dentate precursor cells in *Dfl*^{+/+} mice also show migration deficits.

Previous studies indicate that the formation of the hippocampal (HP) dentate gyrus (DG) requires Cxcr4/Cxcl12 signaling (21-23). Immunohistochemical and *in situ* hybridization analysis showed the decreased expression of Cxcr4 but not Cxcl12 in the *Dfl*^{+/+} embryonic HP [genotype, $F_{1,4}=7.84$, $p=0.049$ (n=3, embryos) (ANOVA)] (**Fig.2A** and **Supplementary Fig.3**). Furthermore, stereological analysis showed a statistically significant volume reduction in the DG, but not in the HP, of perinatal *Dfl*^{+/+} mice [DG: $p=0.0069$, HP: $p=0.36$ (n=4 mice) (Student's t test)] (**Supplementary Fig.4 A**).

During development, neuronal precursors of dentate granule cells migrate to the subpial zone of the DG from the dentate ventricular zone (dVZ) through the fimbrio-dentate junction (FDJ) (**Fig.2B**). The precursors in the subpial zone then proliferate and generate a large number of DG granule cells during the first month of postnatal life (21, 22). We first analyzed cell proliferation following a single injection of BrdU at E18.5 2 h before sacrifice. The number of BrdU-positive cells was 50% lower in *Dfl*^{+/+} mice compared to control mice specifically in the DG but not in the dVZ or the FDJ [genotype, $F_{1,8}=9.82$, $p=0.014$ (n=4-6, embryos) (ANOVA)] (**Fig.2C**). The decreased proliferation in the E18.5 DG could be caused by the decreased generation of dentate precursors in the dVZ or by a migration defect from the dVZ to the DG. To distinguish between these two possibilities, we examined the generation of dentate precursors in earlier developmental stages using BrdU. No difference was observed in the number of BrdU-positive cells in the dVZ at E15.5 and E16.5 (**Supplementary Fig.5A, B**). Additionally, neither Wnt3a nor Lef1 was affected in *Dfl*^{+/+} mice, although Wnt signaling is known to be essential for the proliferation of dentate precursors (**Supplementary Fig.5C, D**) (24). These results support the hypothesis that the generation of dentate precursors is intact in *Dfl*^{+/+} mice.

We next examined the effects of 22q11-related region deficiency on the migration of dentate precursors. To trace the migrating dentate precursors, we performed a BrdU pulse experiment. We injected BrdU at E15.5 and performed the analysis at E18.5. A drastic decrease in the number of BrdU-positive cells was observed in the DG

of *Dfl*/+ mice compared to control mice, but not in the dVZ and the FDJ [genotype x region interaction, $F_{2,8}=40.26$, $p=0.0001$ ($n=3$, embryos) (ANOVA)] (**Fig.2D**). The altered distribution of BrdU-positive cells was also observed at a more caudal level [genotype x region interaction, $F_{2,8}=8.21$, $p=0.012$ ($n=3$ embryos) (ANOVA)] (**Fig.2E**). These results suggest that the migration of dentate precursors to the DG may be delayed. Furthermore, immunohistochemical analysis of Nestin and Prox1 in the DG of *Dfl*/+ mice showed widely dispersed Nestin-positive precursors in the DG (**Supplementary Fig.6**). In contrast, Nestin-positive dentate precursor cells and Prox1-positive granule cells formed different layered organizations (**Supplementary Fig.6**). Taken together, these data show that haplodeficiency of the 22q11-related region caused the migration deficits of dentate precursors to the DG subpial zone.

Hippocampal dentate precursor cells in *Dfl*/+ mice also aberrantly respond to Cxcl12.

To directly examine whether *Cxcr4*/*Cxcl12* signaling deficits cause DG developmental abnormalities, we performed a transwell migration assay using P0 *Dfl*/+ DG-derived cells and *Cxcl12*. Dose response studies showed a typical biphasic response in control DG-derived cells with a peak at 0.1 $\mu\text{g/ml}$ of *Cxcl12*. In contrast, *Dfl*/+ DG-derived cells showed a lower chemotactic response to *Cxcl12* with a peak at 1 $\mu\text{g/ml}$ [dose x genotype interaction, $F_{3,39}=4.03$, $p=0.014$ ($n=7-8$) (ANOVA)] (**Supplementary Fig.7A**). Finally, to test if the migration of *Dfl*/+ dentate precursors is reduced in a more physiological condition, we cocultured E17.5 dVZ explants with aggregates of *Cxcl12*-expressing 293T cells in Matrigel matrices. *Dfl*/+ dVZ-derived cells exhibited a decreased response to *Cxcl12* compared with control dVZ-derived cells [genotype, $F_{1,10}=5.51$, $p=0.041$ ($n=5-7$, embryos) (ANOVA)] (**Supplementary Fig.7B**). The migration of control dVZ-derived cells is *Cxcr4*-dependent, for a *Cxcr4* inhibitor, AMD3100, inhibited migration [treatment, $F_{2,6}=20.18$, $p=0.0022$ ($n=3$, embryos) (ANOVA)] (**Supplementary Fig.8A, B**). Thus, microdeletion of the 22q11-related region caused *Cxcr4*/*Cxcl12* signaling deficits in dentate precursor cells.

***Dgcr8* rescued the reduced responsiveness of *Dfl*/+ MGE-derived cells to *Cxcl12*.**

To identify the gene, or genes, in the 22q11-related region that is responsible for the migration deficits observed in *Dfl/+* mice, we performed a stripe choice assay. Dissociated E13.5 MGE cells obtained from *Dfl/+* and control mice were infected by EGFP-expressing lentivirus and then given a chance to migrate on top of alternating stripes of 293T cells non-transfected or transfected with dsRed and *Cxcl12* (**Fig. 3A**). Their final position was identified by the fluorescence of EGFP 48 h later. *Dfl/+* MGE-derived cells showed a decreased preference for *Cxcl12*-expressing cells compared to non-transfected cell stripes [genotype, $F_{1,18}=5.55$, $p=0.03$, virus, $F_{1,18}=10.16$, $p=0.005$ ($n=4-7$ embryos) (ANOVA)] (**Fig. 3B, C**). For rescue experiments, we utilized lentiviral vectors to express a 22q11-related gene, *Gnb11*, *Zdhhc8* or *Dgcr8*, with EGFP. Only *Dgcr8* significantly restored the decreased preference of *Dfl/+* MGE-derived cells for *Cxcl12* [treatment, $F_{1,18}=10.158$, $p=0.0051$ ($n=4-7$, embryos) (ANOVA)] (**Fig. 3B**). To test whether *Cxcr4*-mediated signaling is normalized by *Dgcr8* or *Cxcr4* overexpression, we measured the *Cxcl12*-induced increase in intracellular calcium ($[Ca^{2+}]_i$) by Rhod3 Ca^{2+} imaging experiments (**Fig. 3D, E**). We applied various concentrations of *Cxcl12* to E13.5 *Dfl/+* MGE-derived neural progenitor cells. The $[Ca^{2+}]_i$ responses to *Cxcl12* was significantly decreased in *Dfl/+* neural progenitors compared with control neural progenitors [genotype, $F_{1,8}=12.82$, $p=0.0072$ ($n=5$, embryos) (ANOVA)]. Both *Dgcr8* and *Cxcr4* rescued this deficit in $[Ca^{2+}]_i$ response to *Cxcl12* of *Dfl/+* MGE-derived neural progenitor cells [genotype, $F_{2,15}=6.27$, $p=0.011$ ($n=5-7$, embryos) (ANOVA), *Dgcr8*: $p=0.0032$, *Cxcr4*: $p=0.0283$ (Fisher's LSD test)].

Finally, to examine whether *Dgcr8* or *Cxcr4* overexpression is sufficient to rescue the migration deficits of *Dfl/+* MGE-derived interneurons, we used a slice tissue culture assay. Brain slices were prepared from E13.5 embryos of *Dfl/+* and wild type mice. Lentiviruses, which express GFP with or without *Dgcr8* or *Cxcr4*, were injected into the MGE (**Fig. 3F**). Three days after control GFP-expressing lentiviral infection, a decreased number of GFP+ cells were observed in the cortex of *Dfl/+* brain slices. In contrast, either *Dgcr8* or *Cxcr4* overexpression at least partially rescued the number of GFP-positive cells in the cortex of *Dfl/+* brain slices (**Fig. 3F, G**). Taken together, our data suggests that interneuron migration deficits in *Dfl/+* mice are caused by *Cxcr4/Cxcl12* signaling deficits and we show that their decreased responsiveness to *Cxcl12* can be rescued by the

overexpression of *Dgcr8*.

Changes in downstream targets of *Dgcr8* in the *Dfl/+* MGE.

miR-200a and miR-224 have been reported to increase *Cxcr4* expression (25, 26). Thus, we examined the expression of these miRNAs in the MGE of E13.5 *Dfl/+* mice by quantitative real time RT-PCR. miR-200a was decreased in the *Dfl/+* MGE, whereas miR-224 was not affected [miR-200a, $p=0.026$; miR-224, $p=0.93$ ($n=3$, embryos) (Student's *t* test)] (**Supplementary Fig.9A**). To determine whether loss of miR-200a causes *Cxcr4* down-regulation in MGE-derived neural progenitors, we utilized LNA miRNA inhibitors. MGE-derived neural progenitors were transfected with anti-miR-200a or anti-miR-224. Anti-miR200a but not anti-miR224 down-regulated *Cxcr4* expression 3 days after transfection compared with a negative control inhibitor (**Supplementary Fig.9B**). The decreased level of miR-200a may be partially responsible for the *Cxcr4/Cxcl12* signaling deficits in *Dfl/+* mice.

Defects in migration of MGE-derived cells and dentate precursor cells in mice of *Dgcr8* haploinsufficiency

To examine whether *Dgcr8* haploinsufficiency affects the development of cortical interneurons and the DG, we analyzed the neurodevelopment of *Dgcr8* heterozygous mice. Immunohistochemical analysis of *Lhx6* and *Gad67* revealed that the distribution of interneurons was also altered in the E18.5 *Dgcr8^{+/-}* cortex [*Lhx6*, layer x genotype interaction, $F_{4,24}=4.21$, $P=0.01$ ($n=4$, embryos); *Gad67*, layer x genotype interaction, $F_{4,16}=5.74$, $p=0.0046$ ($n=3$ embryos) (ANOVA)] (**Fig.1A, B, Supplementary Fig.1B, C**). *Cxcr4* expression is also decreased in the E18.5 *Dgcr8^{+/-}* cortex [genotype, $F_{1,4}=19.50$, $p=0.012$ ($n=3$) (ANOVA)] (**Fig.1C, D**). E13.5 *Dgcr8^{+/-}* MGE-derived cells also showed decreased responsiveness to *Cxcl12* when cocultured with *Cxcl12*-expressing 293T cells [genotype, $F_{1,7}=11.34$, $p=0.011$ ($n=3-6$, embryos) (ANOVA)] (**Fig.1I, J**).

Like the *Dfl/+* mice, the volume of the DG of P0 *Dgcr8^{+/-}* mice is decreased [$P=0.036$, ($n=6$ mice) (Student's *t* test)] (**Supplementary Fig.4B**). A BrdU pulse experiment showed migration deficits of dentate precursor cells in the *Dgcr8^{+/-}* HP [genotype x region interaction, rostral, $F_{2,8}=9.77$, $p=0.0071$ ($n=3$, embryos);

caudal, $F_{2,8}=9.42$, $p=0.0079$ ($n=3$, embryos) (ANOVA)] (**Fig.2D, E**), which was also confirmed by ectopic Nestin-positive precursors (**Supplementary Fig.6**). E17.5 *Dgcr8*^{+/-} dVZ-derived cells exhibited a decreased response to Cxcl12 [genotype, $F_{1,4}=9.19$, $p=0.039$ ($n=3$, embryos) (ANOVA)] (**Supplementary Fig.7C**), although the reduced Cxcr4 expression in the E18.0 *Dgcr8*^{+/-} HP was not statistically significant [genotype, $F_{1,4}=3.57$, $p=0.13$ ($n=3$, mice) (ANOVA)] (**Fig.2A**). Taken together, these data suggest that *Dgcr8* is essential for the normal migration of cortical MGE-derived cells and hippocampal dentate precursor cells.

CXCL12 is reduced in the neuronal layers of the olfactory epithelium in patients with SZ.

The above data suggest the significance of *Dgcr8* and its downstream Cxcr4/Cxcl12 signaling in the developmental abnormalities in a 22q11DS mouse model. Next, we examined if this molecular pathway might be altered in neuronal cells in patients with SZ. It is very difficult to obtain neurons or neuronal cells from living subjects. However, via nasal biopsy combined with laser-capture microdissection, we can obtain neuronal layers of the olfactory epithelium (27). By using this methodology, we compared the expression of CXCR4, CXCL12, and DGCR8 in the neuronal layers of the olfactory epithelium between normal controls and sporadic cases of SZ. The demographic summary is presented in (**Fig.4 A**). We observed a significant reduction in the expression of CXCL12 in patients with SZ compared with normal controls, whereas no difference was observed in the expression of CXCR4 or DGCR8 between these two groups (**Fig.4 B, C**). A significant difference in the expression of CXCL12 in sporadic cases of SZ compared to matched normal controls suggests that the CXCR4/CXCL12 pathway may contribute to the pathophysiology of SZ and be disturbed in a substantial subgroup diagnosed with SZ.

Discussion

The main findings of the present study are as follows: we demonstrated that the haplodeletion of eighteen orthologues of the human genes in the 22q11.2 region (*Df1/+* mice) cause defects in cortical interneuron migration and hippocampal dentate precursor migration, and shows functional abnormalities in *Cxcr4/Cxcl12* signaling. This study is the first that directly links the 22q11 microdeletion and these developmental abnormalities via a *Cxcr4/Cxcl12* signaling deficiency. With multiple lines of evidence, we proved that *Dgcr8* in the 22q11 region might play, at least in part, a role as an upstream master regulator. In parallel, in microdissection of human neuronal tissues via nasal biopsy, we showed that CXCL12 expression was significantly decreased in sporadic SZ patients compared with normal controls. Although it is unlikely, we acknowledge that the CXCL12 signal may also come from non-neuronal cells, such as macrophages and sustentacular cells.

Our findings are consistent with a recent study by Meechan et al (10), in which the disturbances in the placement of PV-interneurons and the reduced expression of the *Cxcr4* were reported in another mouse model of 22q11DS (*LgDel/+* mice). In the present study, by using rescue experiments of *Df1/+* interneuron migration, we could pin down the pivotal role of *Dgcr8*-mediated miRNA regulation in the downstream phenotypes of 22q11 deletion, including *Cxcr4/Cxcl12* functional deficits. miRNA-mediated regulation can buffer increases or reductions in gene dosage (28, 29). Haploinsufficiency of *Dgcr8* might disrupt miRNA-mediated buffering effects, and uncovers the effects of 22q11 microdeletion as well as biological or environmental perturbations. This study will open a window to study *Cxcr4/Cxcl12* functional deficits more mechanistically in the context of 22q11DS, in particular in the link of *Dgcr8*.

Although 22q11DS accounts for only a very small subset of SZ, we found significant reduction of CXCL12 levels, but failed to observe change in DGCR8 levels, in sporadic SZ patients. Of note, in 22q11DS mouse models, *Cxcr4* is affected. We believe that these two positive (changes in either *Cxcr4* or CXCR12) and negative (no change in DGCR8) results are equally important to explore a possible link between 22q11DS and SZ.

The positive results of CXCL12 suggest that Cxcr4/Cxcl12 signaling deficits observed in 22q11DS mouse models may have some relevance in SZ pathophysiology. DGCR8 may underlie an upstream etiology for aberrant CXCR4/CXCL12 signaling deficits in 22q11DS-associated mental manifestation (including SZ-like disturbances). However, this specific etiology may not account for most cases of sporadic SZ. This working hypothesis fits with a well-appreciated notion that SZ is caused by multiple etiologies but has some levels of commonality in the pathophysiology. The proposal from the present study that CXCR4/CXCL12 may underlie a common pathophysiology of SZ may have translational potential, for example aiding biomarker cultivation in SZ and related conditions.

Materials and Methods

The generation of *Df1/+* 22q11DS model mice was previously described (30). The XG058 ES cells (BayGenomics, <http://baygenomics.ucsf.edu>) were used to generate *Dgcr8^{+/-}* mice. Mice were maintained on the C57Bl6 genetic background for at least eleven generations. Mouse colonies were maintained in accordance with the protocols approved by the Committee on Animal Research at Research Institute, Shiga Medical Center.

Olfactory epithelium (OE) tissues were obtained by nasal biopsy as previously described (27). The full details of subjects and clinical assessment and the analysis of microarray are presented in SI Materials and Methods.

Full descriptions of the volumetric measurement of the hippocampus, as well as descriptions of BrdU labeling analysis, immunohistochemical analysis, *in situ* hybridization, and chemotaxic assay, explants coculture, stripe choice assay, slice culture, neural progenitor cell culture, Ca imaging, miRNA real-time RT PCR, miRNA knockdown studies, real-time RT-PCR are detailed in SI Materials and Methods.

Statistical significance was assessed by unpaired Student's *t* test. All data, unless stated otherwise, are expressed as mean \pm standard deviation (SD). For comparisons of more than two groups, one-way or two-way repeated measures analysis of variance (ANOVA) followed by Fisher's LSD test was used. A probability of less than 5% ($p < 0.05$) was considered statistically significant.

Acknowledgements

This work was supported by JSPS KAKENHI Grant Number 25670154 (K.T.), NOVARTIS Foundation for the Promotion of Science (K.T.), Uehara Memorial Foundation (K.T.), USPHS grants MH-084018 (A.S.), MH-094268 Silvo O. Conte center (A.S.), MH-069853 (A.S.), MH-085226 (A.S.), MH-088753 (A.S.), MH-092443 (A.S.), Stanley (A.S.), RUSK (A.S.), S-R foundations (A.S.), NARSAD (A.S.) and the Maryland Stem Cell Research Fund (A.S.). This project is partly funded by Astellas Pharma (A.S.).

References

1. Pulver AE, *et al.* (1994) Psychotic illness in patients diagnosed with velo-cardio-facial syndrome and their relatives. *J Nerv Ment Dis.* 182(8):476-478.
2. Karayiorgou M, *et al.* (1995) Schizophrenia susceptibility associated with interstitial deletions of chromosome 22q11. *Proc Natl Acad Sci U S A.* 92(17):7612-7616.
3. Manolio TA, *et al.* (2009) Finding the missing heritability of complex diseases. *Nature* 461(7265):747-753.
4. Puech A, *et al.* (1997) Comparative mapping of the human 22q11 chromosomal region and the orthologous region in mice reveals complex changes in gene organization. *Proc Natl Acad Sci U S A* 94(26):14608-14613.
5. Lindsay EA, *et al.* (1999) Congenital heart disease in mice deficient for the DiGeorge syndrome region. *Nature* 401(6751):379-383.
6. Stark KL, *et al.* (2008) Altered brain microRNA biogenesis contributes to phenotypic deficits in a 22q11-deletion mouse model. *Nat Genet* 40(6):751-760.
7. Paylor R & Lindsay E (2006) Mouse models of 22q11 deletion syndrome. *Biol Psychiatry* 59(12):1172-1179.
8. Merscher S, *et al.* (2001) TBX1 is responsible for cardiovascular defects in velo-cardio-facial/DiGeorge syndrome. (Translated from eng) *Cell* 104(4):619-629.
9. Meechan DW, Tucker ES, Maynard TM, & LaMantia AS (2009) Diminished dosage of 22q11 genes disrupts neurogenesis and cortical development in a mouse model of 22q11 deletion/DiGeorge syndrome. *Proc Natl Acad Sci U S A* 106(38):16434-16445.
10. Meechan DW, Tucker ES, Maynard TM, & Lamantia AS (2012) Cxcr4 regulation of interneuron migration is disrupted in 22q11.2 deletion syndrome. *Proc Natl Acad Sci U S A* 109(45):18601-18606.
11. Woo TU, Miller JL, & Lewis DA (1997) Schizophrenia and the parvalbumin-containing class of

- cortical local circuit neurons. *Am J Psychiatry* 154(7):1013-1015.
12. Hashimoto T, *et al.* (2003) Gene expression deficits in a subclass of GABA neurons in the prefrontal cortex of subjects with schizophrenia. *J Neurosci* 23(15):6315-6326.
 13. Kimoto S, *et al.* (2012) Selective overexpression of Comt in prefrontal cortex rescues schizophrenia-like phenotypes in a mouse model of 22q11 deletion syndrome. *Transl Psychiatry* 2:e146.
 14. Fenelon K, *et al.* (2011) Deficiency of Dgcr8, a gene disrupted by the 22q11.2 microdeletion, results in altered short-term plasticity in the prefrontal cortex. *Proc Natl Acad Sci U S A*.
 15. Stumm RK, *et al.* (2003) CXCR4 regulates interneuron migration in the developing neocortex. *J Neurosci* 23(12):5123-5130.
 16. Tiveron MC, *et al.* (2006) Molecular interaction between projection neuron precursors and invading interneurons via stromal-derived factor 1 (CXCL12)/CXCR4 signaling in the cortical subventricular zone/intermediate zone. *J Neurosci* 26(51):13273-13278.
 17. Lopez-Bendito G, *et al.* (2008) Chemokine signaling controls intracortical migration and final distribution of GABAergic interneurons. *J Neurosci* 28(7):1613-1624.
 18. Flames N, *et al.* (2004) Short- and long-range attraction of cortical GABAergic interneurons by neuregulin-1. *Neuron* 44(2):251-261.
 19. Marin O & Rubenstein JL (2003) Cell migration in the forebrain. *Annu Rev Neurosci* 26:441-483.
 20. Wonders CP & Anderson SA (2006) The origin and specification of cortical interneurons. *Nat Rev Neurosci* 7(9):687-696.
 21. Li G, Kataoka H, Coughlin SR, & Pleasure SJ (2009) Identification of a transient subpial neurogenic zone in the developing dentate gyrus and its regulation by Cxcl12 and reelin signaling. *Development* 136(2):327-335.
 22. Bagri A, *et al.* (2002) The chemokine SDF1 regulates migration of dentate granule cells. *Development* 129(18):4249-4260.
 23. Lu M, Grove EA, & Miller RJ (2002) Abnormal development of the hippocampal dentate gyrus in mice lacking the CXCR4 chemokine receptor. *Proc Natl Acad Sci U S A* 99(10):7090-7095.
 24. Lee SM, Tole S, Grove E, & McMahon AP (2000) A local Wnt-3a signal is required for development of the mammalian hippocampus. *Development* 127(3):457-467.
 25. Rosati J, *et al.* (2011) Smad-interacting protein-1 and microRNA 200 family define a nitric oxide-dependent molecular circuitry involved in embryonic stem cell mesendoderm differentiation. *Arterioscler Thromb Vasc Biol* 31(4):898-907.
 26. Huang L, *et al.* (2012) MicroRNA-224 targets RKIP to control cell invasion and expression of metastasis genes in human breast cancer cells. *Biochem Biophys Res Commun* 425(2):127-133.
 27. Tajinda K, *et al.* (2010) Neuronal biomarkers from patients with mental illnesses: a novel method through nasal biopsy combined with laser-captured microdissection. *Mol Psychiatry* 15(3):231-232.
 28. Staton AA, Knaut H, & Giraldez AJ (2011) miRNA regulation of Sdf1 chemokine signaling provides genetic robustness to germ cell migration. *Nat Genet* 43(3):204-211.

29. Herranz H & Cohen SM (2010) MicroRNAs and gene regulatory networks: managing the impact of noise in biological systems. *Genes Dev* 24(13):1339-1344.
30. Paylor R, *et al.* (2001) Mice deleted for the DiGeorge/velocardiofacial syndrome region show abnormal sensorimotor gating and learning and memory impairments. *Hum Mol Genet.* 10(23):2645-2650.

Figure legends

Fig. 1 | Microdeletion of the 22q11-related region reduced the Cxcl12-induced chemotaxis of MGE-derived cells.

(A-D) Immunofluorescence for Lhx6 (red, A), Cxcr4 (red, C) and fluorescent Nissl (green) of coronal sections of E18.5 *Dfl/+*, *Dgcr8^{+/-}* and control cerebral cortices. Quantification of the distribution of marker-positive cells/layer (B) and the relative fluorescent intensity of Cxcr4 per cell (D). Values are the mean±S.D. MZ, marginal zone; sCP, superficial cortical plate; dCP, deep cortical plate; IZ, intermediate zone; VZ/SVZ, ventricular zone/subventricular zone. Scale bar=200 μm.

(E) Quantitative real-time PCR of Cxcr4 in the E15.5 *Dfl/+* cortex. Values have been normalized to β-actin abundance. *p=0.025

(F-J) Schematic of the experimental design (F). Medial ganglionic eminence (MGE) explants of E13.5 *Dfl/+* (G), *Dgcr8^{+/-}* (I) and control embryos were cultured in Matrigel adjacent to Cxcl12-expressing 293T cell aggregates for 60 h. Scale bar=400 μm. The distance migrated by the furthest twenty MGE-derived cells was measured (H, J).

Values are the mean ± S.D. *p=0.0079 (H), *p=0.012 (J).

Fig. 2 | *Dfl/+* and *Dgcr8^{+/-}* hippocampal dentate precursor cells exhibit decreased responses to Cxcl12.

(A) Immunofluorescence of the *Dfl/+*, *Dgcr8^{+/-}* and control E18.5 hippocampus for Cxcr4 (green) and fluorescent Nissl (blue). Quantification of the relative fluorescent intensity of Cxcr4 per cell (right). Values are the mean ± S.D. Scale bar=200 μm.

(B) Schematic representation of the progressive development of dentate neuronal progenitor cells.

(C) Representative images of immunofluorescent studies on the *Dfl*/+ and control E18.5 hippocampus for BrdU (green) and DAPI staining of nuclei (blue) (left). BrdU was administrated 2hrs before sacrificing. The number of BrdU-positive cells is reduced in the dentate gyrus (DG), but not in the dentate ventricular zone (VZ) and fimbrio-dentate junction (FDJ) of *Dfl*/+ mice (right). Data are shown as mean±S.D. Scale bar=100µm.

(D-E) Representative immunofluorescent images of the *Dfl*/+, *Dgcr8*^{+/-} and control E18.5 hippocampus for BrdU (green) and DAPI staining of nuclei (blue) at rostral (D) and caudal levels (E) (left). BrdU was administrated at E15.5 and sacrificed at E18.5. The distribution of BrdU-positive cells is altered in the *Dfl*/+ and *Dgcr8*^{+/-} hippocampus (right). Data are shown as mean±S.D. Scale bar=200 µm.

Fig.3 | The chemotactic deficits of *Dfl*/+ MGE-derived cells are restored by lentivirus-mediated reintroduction of *Dgcr8*.

(A) Schematic of the experimental design. MGE-derived cells from *Dfl*/+ and control embryos were infected by GFP-expressing lentivirus and plated on top of alternating stripes of 293 T cells nontransfected and transfected with dsRed and *Cxcl12*. The distribution of MGE-derived cells was assessed 48hours later.

(B) Distribution of EGFP-positive MGE-derived cells from E13.5 *Dfl*/+ and control embryos. For rescue experiments, *Gnb11*, *Zdhhc8* or *Dgcr8* with EGFP were introduced by lentivirus. The dotted lines indicate the boundary between nontransfected and transfected 293T cells. Scale bar=200µm. Values are the mean±S.D.

(C) Quantification of the percentage of MGE-derived cells on *Cxcl12*-expressing 293T cells. Values are the mean±S.D. *p=0.03

(D-E) Representative example of [Ca²⁺]_i response after *Cxcl12* addition in *Dfl*/+ and control MGE-derived neuronal progenitors. For rescue experiments, *Dgcr8* or *Cxcr4* with EGFP were introduced by lentivirus.

Averaged data for the concentration-dependent effect of *Cxcl12* on [Ca²⁺]_i responses (E). Error bars represent the SEM.

(F-G) Schematic of the experimental paradigm used to analyze the effects of *Dgcr8* or *Cxcr4* overexpression on the migration deficits of MGE-derived interneurons from *Dfl*/+ mice (F). Brain slice cultures were prepared

from *Dfl/+* and control E13.5 embryos. *Dgcr8* or *Cxcr4* with EGFP were introduced by lentivirus. Dotted lines represent the pallial/subpallial boundary. Note the decreased migration from the MGE to *Ncx* (neocortex) in *Dfl/+* mice and the partial rescue of this migration deficit by *Dgcr8* and *Cxcr4* 72 hrs after infection. Scale bar=300 μm .

Fig.4 | CXCL12 is decreased in the olfactory neuronal layer in patients with SZ.

(A) Demographics of human subjects in this study. a, ANOVA; b, Fisher's exact test.

(B) Microarray analysis of *DGCR8*, *CXCR4* and *CXCL12* expression in the laser-capture microdissected neuronal layer of the olfactory epithelium from control and SZ subjects. a, ANOVA.

(C) The expression level of *CXCL12* for each control (circles) and SZ (squares) subject. The results of each probe are shown separately and correspond with the Affymetrix probeset ID show in B. * $p=0.001$, ** $p=0.036$.

Fig1

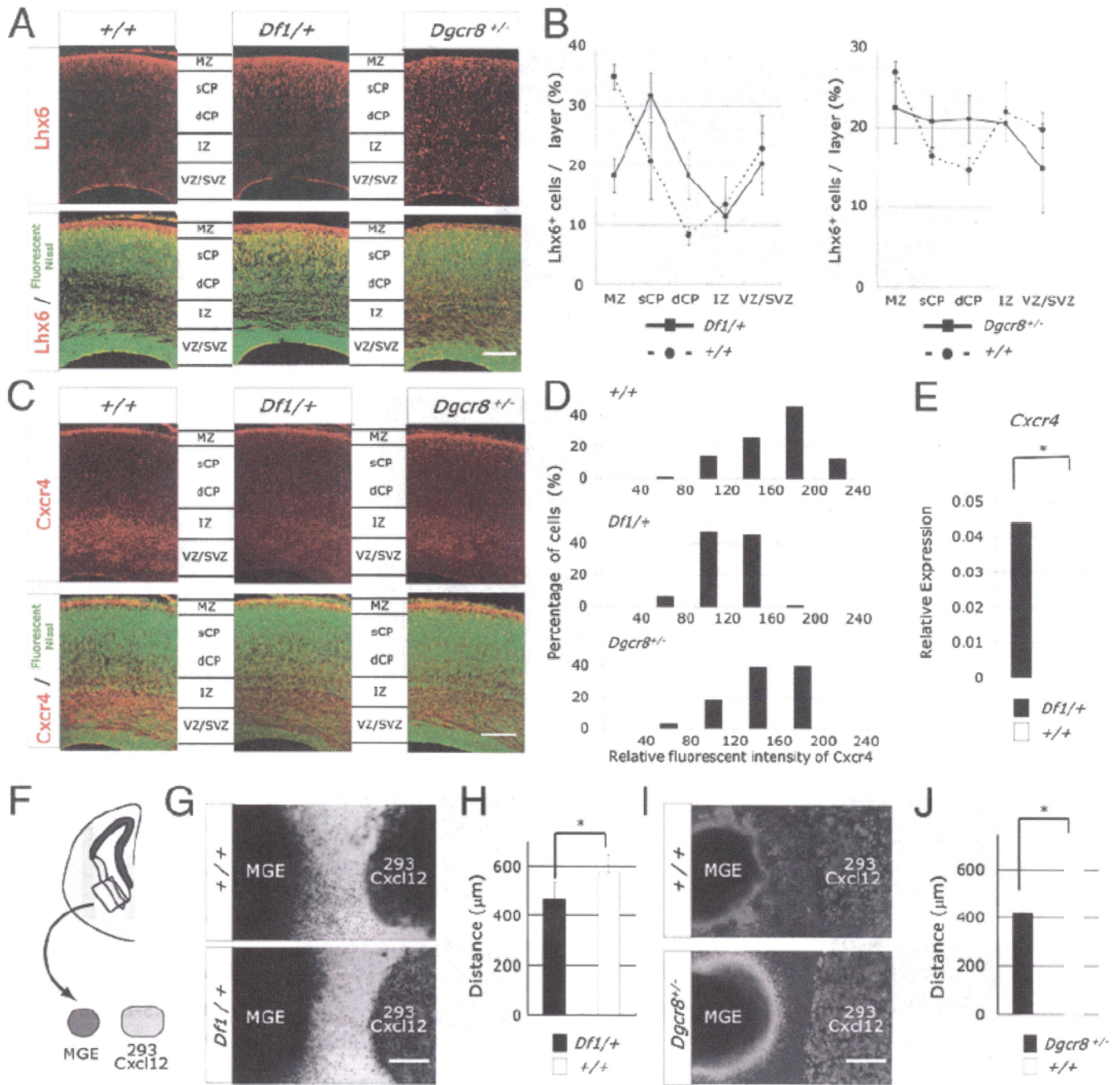


Fig2

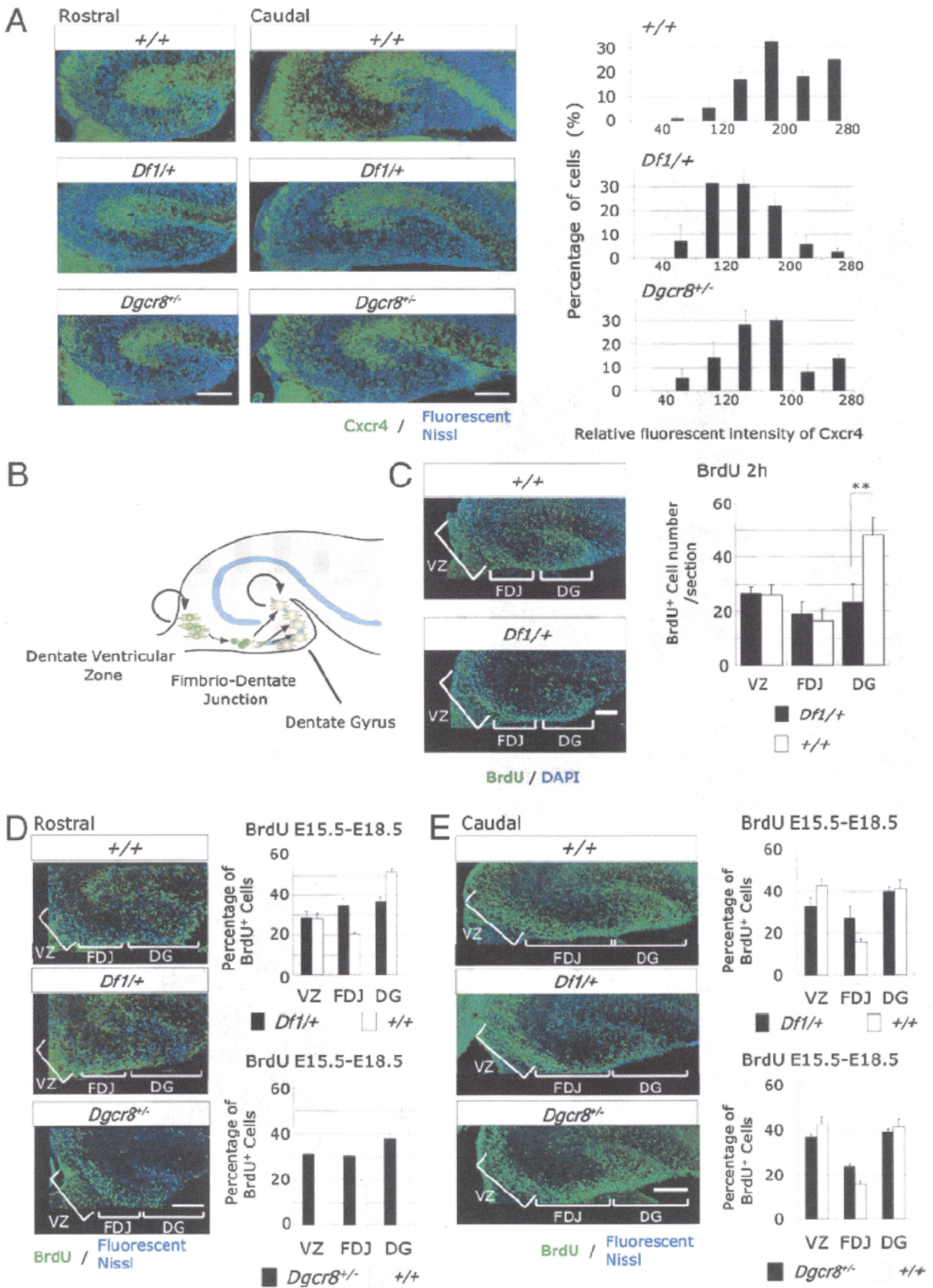


Fig3

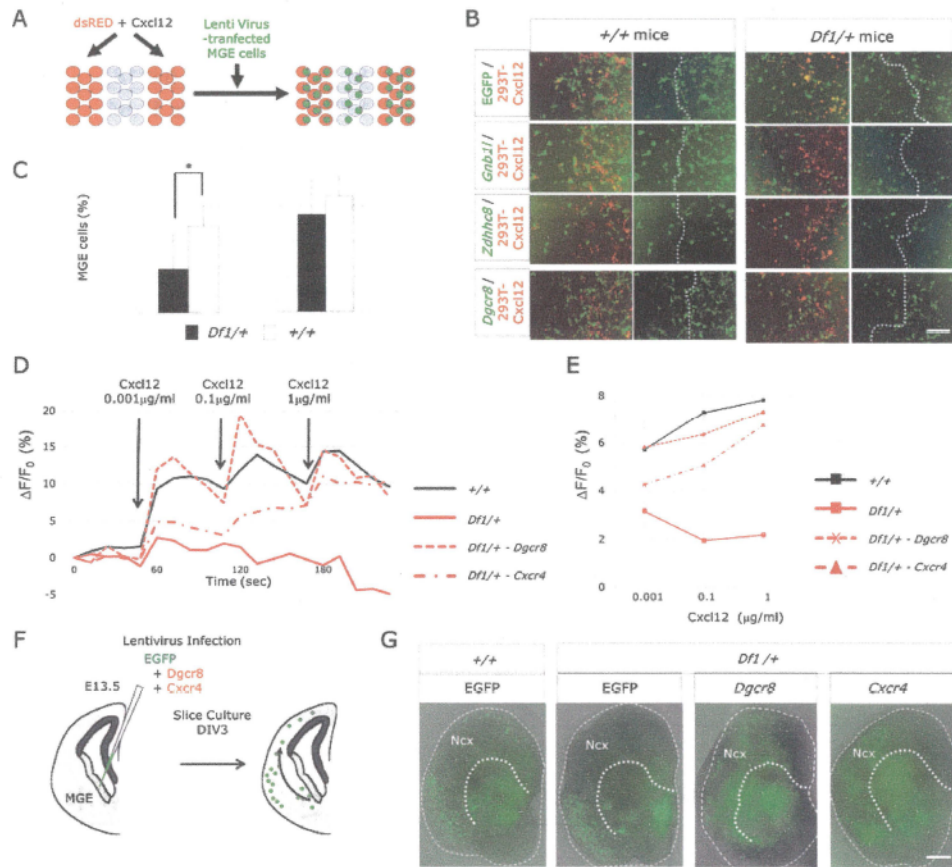


Fig4

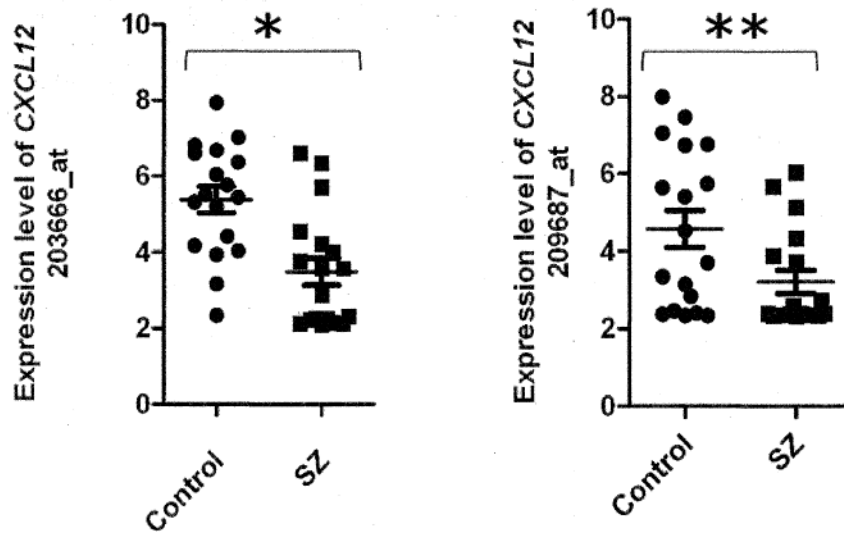
A

Characteristics	SZ (N=18)	Control (N=18)	p value
Age (years, Average \pm SD)	38.78 \pm 11.79	39.17 \pm 11.84	0.921 ^a
Sex (male/female)	12/6	14/ 4	0.711 ^b
SANS (total, Average \pm SD)	7.79 \pm 4.92		
SAPS (total, Average \pm SD)	4.26 \pm 3.67		

B

Gene Symbol	Gene Title	Affymetrix Probeset ID	Fold-Change	p-value ^a
DGCR8	DiGeorge syndrome critical region gene 8	219811_at	-1.24	0.083
		218650_at	-1.47	0.173
		64474_g_at	-1.25	0.245
		91617_at	-1.32	0.406
CXCR4	chemokine (C-X-C motif) receptor 4	217028_at	-1.22	0.088
		211919_s_at	-1.33	0.293
		209201_x_at	-1.17	0.567
CXCL12	chemokine (C-X-C motif) ligand 12	203666_at	-3.43	0.001
		209687_at	-2.29	0.036

C



Supplementary Figure Legends

Supplementary Fig.1 | Abnormal distribution of Gad67⁺ cells in the cortices of *Dfl*/⁺ and *Dgcr8*^{+/-} mice.

(A) A partial map of the mouse 22q11-related region on chromosome 16.

The line below the map indicates the deleted region in *Dfl*/⁺ mice.

(B-C) Immunofluorescence for Gad67 (red, A) and fluorescent Nissl (green) of coronal sections of E18.5 *Dfl*/⁺, *Dgcr8*^{+/-} and control cerebral cortices. Quantification of the distribution of marker-positive cells/layer (B). Values are the mean±S.D. MZ, marginal zone; sCP, superficial cortical plate; dCP, deep cortical plate; IZ, intermediate zone; VZ/SVZ, ventricular zone/subventricular zone. Scale bar=200 μm.

Supplementary Fig.2 | No abnormalities in the expression of Neuregulin/ErbB4 signaling-related genes in *Dfl*/⁺ mice.

Quantitative real-time RT-PCR of Neuregulin1, Neuregulin3 and ErbB4 in E13.5 *Dfl*/⁺ MGE and E15.5 *Dfl*/⁺ cortex. Values have been normalized to β-actin abundance.

Supplementary Fig.3 | Microdeletion of the 22q11-related region reduced *Cxcr4* expression in the hippocampus.

In situ hybridization of *Cxcl12* and *Cxcr4* in the hippocampus of *Dfl*/⁺ and control mice at E15.5. Scale bar=200μm.

Supplementary Fig.4 | Reduced volume of the hippocampal dentate gyrus in *Dfl*/⁺ and

***Dgcr8*^{+/-} mice.**

The reduction in the volume of the dentate gyrus, but not hippocampus proper, of P0 *Dfl/+* mice was measured by stereology. Data are shown as mean±S.D. *p=0.0069 (A), *p=0.036 (B)

Supplementary Fig.5 | The intact proliferation of dentate progenitors in the embryonic hippocampus of *Dfl/+* mice.

(A) Representative images of sections processed for fluorescent immunostaining of BrdU. BrdU was administrated 2hour before sacrificing at E15.5 or E16.5.

(B) The number of BrdU+ cells in the dentate ventricular zone of *Dfl/+* and control mice. BrdU was administrated 2hour before sacrificing at E15.5 or E16.5. Data are shown as mean±S.D.

(C) In situ hybridization of Wnt3a and Lef1 in the hippocampus of *Dfl/+* and control mice at E15.5. Arrows indicated the sites of Wnt3a expression. Scale bar=200µm.

(D) Quantitative real-time RT-PCR of Wnt3a and Lef1 in the E15.5 *Dfl/+* hippocampus. Values have been normalized to β-actin abundance.

Supplementary Fig.6 | Abnormal distribution of dentate progenitors in the embryonic hippocampus of in *Dfl/+* and *Dgcr8*^{+/-} mice.

Immunofluorescence for Nestin (red), Prox1 (green), and fluorescent Nissl (blue) of the hippocampus of E18.5 *Dfl/+*, *Dgcr8*^{+/-} and control mice. Arrows indicate ectopic Nestin-positive cells. Scale bar= 200 µm.

Supplementary Fig.7 | *Dfl/+* and *Dgcr8*^{+/-} hippocampal dentate precursor cells exhibit decreased responses to Cxcl12.

(A) Chemotactic response of P0 DG-derived cells from *Dfl/+* and control mice to increasing

concentrations of Cxcl12 in vitro. Data are shown as mean±S.D..

(B-C) Dentate ventricular zone (dVZ) explants from the hippocampus of E17.5 *Dfl/+* (B), *Dgcr8^{+/-}* (C) and control embryos were cultured in Matrigel adjacent to Cxcl12-expressing 293T cell aggregates for 100 hrs (left). Scale bar=400µm. The distance migrated by the furthest twenty dVZ-derived cells was measured (right). Values are the mean±S.D. *p=0.041 (B), *p=0.039 (C)

Supplementary Fig.8 | Cxcl12-dependent migration of dentate ventricular zone-derived cells.

Dentate ventricular zone (dVZ) explants from the hippocampus of E17.5 wild type embryos were cultured in Matrigel adjacent to Cxcl12-expressing 293T cell aggregates for 100 hours with or without a Cxcr4 inhibitor, AMD3100 (30µM) (A). Scale bar=400µm. The distance migrated by the furthest twenty dVZ-derived cells was measured (B). Values are the mean ± S.D. *p=0.0022

Supplementary Fig.9 | The miRNA abnormality in *Dfl/+* MGE and its effects on Cxcr4 expression.

(A) Quantitative real-time RT-PCR analysis of miR-200a and miR-224 in the E13.5 *Dfl/+* and control MGE. Values have been normalized to SNORD 96A abundance. *p=0.027

(B) Inhibition of miR-200a but not miR-224 decreased Cxcr4 expression in MGE-derived neural progenitors. MGE-derived neural progenitors were isolated from E13.5 mouse embryos and transfected with miRNA inhibitors. Immunofluorescent staining was performed 3days after transfection. Representative images are shown. Scale bar=100µm.

SI Materials and Methods

Volumetric measurement of the hippocampus

Mice were perfused through the heart with phosphate buffered saline followed by formaline and fixed for 24hours. Brain tissue was subsequently embedded in celloidin. Sections were taken at approximately 40 μ m thickness using a sliding microtome and stained using cresyl violet. Images of serial sections through the entire hippocampus from P0 mice were analyzed in Image-J. The interval between adjacent sections on each slide was 120 μ m. Volume was determined by the Cavalieri method. Borders of the hippocampus, excluding the subiculum but including the fimbria and dentate gyrus, were traced manually followed by manual tracing of the dentate gyrus alone. Finally, areas of the hippocampus proper and the granule cell layer of the dentate gyrus were measured bilaterally for all cases.

BrdU labeling analysis

We injected pregnant mice intraperitoneally with BrdU (100mg/Kg). Cryostat sections were prepared as described above. For the quantification of the number of proliferating cells, serial sections were photographed, and six equivalent sections of *Dfl/+* or *Dgcr8^{+/-}* and control mice were used to count BrdU-positive cells in the dentate ventricular zone, fimbrio-dentate junction and dentate gyrus.

Immunohistochemistry of tissue sections

Immunohistochemical staining was performed with primary antibodies for 24hours at 4°C after blocking for 30min at room temperature with 5% donkey serum (Chemicon).

The cryostat sections were incubated for 1 hour at room temperature with secondary antibodies and fluorescent Nissl (Molecular Probes, Eugene, OR). The primary antibodies used were anti-BrdU (BU1/75, Oxford Biotechnology), anti-Prox1 (Covance), anti-Nestin (Chemicon), anti-Gad67 (Chemicon) and anti-Lhx6 (AVIVA Systems Biology). The distribution of Lhx6-positive or Gad67-positive cells was estimated as previously described(1). Slides were examined with an Olympus confocal laser scanning microscope (FV-300, Olympus).

In situ hybridization

In situ hybridization experiments were performed using digoxigenin riboprobes on 12µm frozen sections. Slides were fixed in 4% PFA and 0.2% gluteraldehyde for 10 min and treated with proteinase K (10µg/ml) for 3 min. Slides were incubated with hybridization buffer for 2hours at 70°C, followed by overnight incubation with a digoxigenin-labeled probe at 70°C. Six washes were performed as follows: 50% formamide, 6× SSC at 70°C for 15min three times and 50% formamide, 2.4× SSC at 65°C for 15min three times. Slides were then incubated with horseradish alkaline phosphatase-conjugated anti-digoxigenin and NBT (nitroblue tetrazolium)/BCIP (5-bromo-4-chloro-indolyl phosphate) for signal detection. The probes used were as follows: *Wnt3a* (GenBank accession no. BC152754), *Lef1*(GenBank accession no. BC057543), *Cxcl12* (GenBank accession no. BC046827) and *Cxcr4* (GenBank accession no. BC031665).

Chemotaxis Assay

The hippocampal DGs were removed from pups of *Dfl/+* and control mice at postnatal

day 0, and dissociated using a papain-neural dissociation kit (Miltenyi Biotec GmbH, Bergisch. Gladbach, Germany). The migration of DG-derived cells was studied using a cell culture PET membrane insert (Becton Dickinson, NJ, USA) containing 8.0 μm pores, coated with 20 $\mu\text{g}/\text{ml}$ laminin. For chemotaxis, increasing concentrations of Cxcl12 (Peprotech) ranging from 1ng/ml to 1 $\mu\text{g}/\text{ml}$ were added to the bottom compartment of the chemotaxis chamber, and 10⁶cells/ml in Neurobasal medium (Gibco) with 2% B27 supplement, 0.5% glucose and 2mM L-glutamine was added to the upper compartment of each well. The chemotactic responses of hippocampal DG-derived cells were determined after 24hours by counting migrating cells in five high-powered fields.

Hippocampal Dentate VZ and MGE Explants coculture

Dentate VZ and MGE explants were dissected out from organotypic slices of E17.5 and E13.5 *Df1/+* and control mouse embryos, respectively. The explants were confronted with 293T cell aggregates expressing DsRed (Mock) or DsRed and Cxcl12 and were cultured in Matrigel (BD Biosciences, San Jose, CA) diluted 1:1 with Neurobasal medium (Invitrogen, SanDiego, CA) supplemented with 2% B27 supplement (Gibco, Grand Island, NY). For the quantification, the distance migrated by the 20 furthest cells from the explants was quantified.

Cloning and production of lentiviral vectors.

Cytomegalovirus (CMV)-IE / chicken β -actin promoter (CAG), IRES-EGFP and *Dgcr8* or *Gnb11* or *Zdhhc8* were introduced to pLenti6.4 lentiviral vector (Invitrogen) and lentiviruses were produced as previously described (2, 3). Briefly, 293T cells were transfected using lipofectamine 2000 (Invitrogen) with the lenriviral vector and two

helper, Δ 8.9 and VSVG plasmids. After 48 hours, the supernatants were spun at 83,000 xg for 1.5 h, and the pellet was resuspended in 100 μ l of PBS.

Stripe Choice Assay

293T cells were plated in a 4 cell chamber slide coated with Matrigel (BD Biosciences, San Jose, CA) and transfected with dsRed and Cxcl12 expression vectors. After an overnight incubation, transfected cells were removed with a pipette tip (one line every 2-3mm to make stripes). Nontransfected 293T cells were plated on top and allowed to attach to the empty stripes for 2hours. After the unattached cells were washed out with PBS, lentivirus-infected dissociated MGE-derived cells from E13.5 *Dfl/+* and control embryos were added on top. The distribution of the MGE-derived cells was identified by the fluorescence of lentivirus-mediated EGFP expression 48hours after plating.

Slice Culture

Brain slice cultures were prepared from the E13.5 embryonic mouse telencephalon. The 300 μ m coronal cortical sections were prepared by cutting on a vibrating microtome (VT1000S, Leica, Nussloch, Germany). Slices were cultured on Millicell-CM (Biopore PICMORG50, Millipore) in organ tissue dishes containing 1.2 ml of medium (Neurobasal/B-27 with glutamine and 5% fetal calf serum and 1% penicillin/streptomycin (Life Technologies)). Slices were allowed to recover for 1-2hours before lentiviral injection. Analysis was performed after a 3-day culture at 37°C with 5% CO₂.

Neural progenitor cell culture

Neural progenitor cell cultures were established from the medial ganglionic eminence of E13.5 mouse embryos. Tissues were dissociated by trituration with a fire-polished Pasteur pipette. Cells were cultured in Neurobasal/B-27 with glutamine and 5% fetal calf serum and 1% penicillin/streptomycin (Life Technologies).

Ca imaging

The neuronal progenitors were prepared from the medial ganglionic eminence at E13.5 and plated onto Matrigel-coated glass bottom dishes. All measurements were performed 3 days after preparation. For measurement of intracellular calcium, primary cultured neuronal progenitors were loaded with 10 μ M

Rhod3 acetoxymethyl ester and 2.5mM probenecid (Rhod3 Imaging Kit, Molecular Probes) at 37°C for 1hour according to the manufacturer's instructions. Cells were incubated for 30min at 37°C before adding Cxcl12 (R&D Systems, Minneapolis, MN, USA) and then fluorescent images were captured through a Zeiss AxioCam MRm CCD camera and processed using Image-J.

miRNA real-time RT PCR

Total cellular RNA, including miRNA, was extracted from cells using a miRNeasy Mini Kit (QIAGEN, Valencia, CA, USA). Total RNA (200-500ng) was reverse-transcribed with a miScript II RT Kit (QIAGEN). The real-time reverse-transcription polymerase chain reaction (RT-PCR) for the quantification of a subset of miRNAs (miR-200a, and miR-224) was carried out with miScript Primer Assays and a miScript SYBR Green PCR Kit (QIAGEN). Values were normalized to SNORD 96A.

miRNA Knockdown Studies

Fluorescein 5'-isothiocyanate-labeled miRCURY LNA miRNA Power Inhibitors (Exiqon, Woburn, MA, USA) were obtained to inhibit miR-200a, miR-224, or negative control with no known mouse sequence homology (Negative Control A). LNA Power Inhibitors were transfected using a NEPA21 electroporator (Nepagene, Chiba, Japan). Dissociated mouse MGE-derived neural progenitors were centrifuged at 90xg for 5 min at 4°C and resuspended in a 100µl mixture of Opti-MEM (Invitrogen) and 150pmol LNA Power Inhibitor. Two types of electric pulses were applied to the mixture. Poring pulse condition: 275V; pulse length, 0.5ms; two pulses; interval between the pulses, 50ms; decay, 10%; rate with + polarity. The transfer pulse condition: 20V; pulse length, 50ms; five pulses; interval between the pulses, 50ms; decay, 40%; rate with +/- polarity. After the electroporation, cells were immediately seeded onto a Matrigel-coated slide chamber (Nunc, Naperville, IL). 3days after the electroporation, cells were fixed for immunocytochemistry.

Real-time RT-PCR

Total cellular RNA was extracted from cells using a RNeasy Mini Kit (QIAGEN, Valencia, CA, USA). Total RNA was reverse-transcribed with a PrimeScript 1st strand cDNA synthesis kit (Takara, Shiga, Japan). Intron spanning *Taqman* probes were designed using the Roche Universal Probe Library method. Amplifications were run in a LightCycler 480 system (Roche). All of the data were analyzed by using β -actin levels as reference.

The following primers were employed: *Cxcr4*, 5'-gtctatgtggcgctctggat-3' and

5'-acgtcggcaaatgaagtc-3', probe: human #63; *Neuregulin1 typeI*:
5'-ggaagggcaagaagaaggac-3' and 5'-cctggcttttcatctctttca-3', probe: human #107;
Neuregulin1 typeIII: 5'-caggaactcagccacaaaca-3' and 5'-cagtcgtggatgtagatgtgg-3' ,
probe: human #68; *Neuregulin3*: 5'-aggaagccagcctatcaagc-3' and
5'-ttcctatgcaacatcccactc-3' , probe: human #26; *ErbB4*: 5'-ctgggggagccttctgat-3' and
5'-ctgttctctgcgcacactg-3' , probe: human #26.

Subjects and clinical assessment

Eighteen subjects with schizophrenia and seventeen age-, gender-, education-, and smoking habit matched normal controls were recruited from our pool of patients and controls that we previously described (4). Patients were recruited from the outpatient psychiatric clinics of the Johns Hopkins Medical Institutions. The diagnosis was performed according to criteria of the Diagnostic and Statistical Manual of Mental Disorders-Fourth Edition (DSM-IV) (American Psychiatric Association APA). Normal controls were recruited from the general population through flyers posted at the Johns Hopkins Hospital and an ad hoc advertisement placed in a local magazine. All subjects were administered the Structured Clinical Interview for DSM-IV Axis I Disorders-Clinician Version (SCID-IV). All patients were assessed with the Scales for the Assessment of Positive and Negative Symptoms (SAPS and SANS) by a study psychiatrist who specializes in schizophrenia. Subjects were excluded from the study if they had a history of traumatic brain injury with loss of consciousness for >1hour, a history of drug abuse within 6 months of the study or drug dependence within 12 months of the study, or a history of untreated major medical illnesses. The study was approved by the Johns Hopkins Institutional Review Board, and all subjects gave

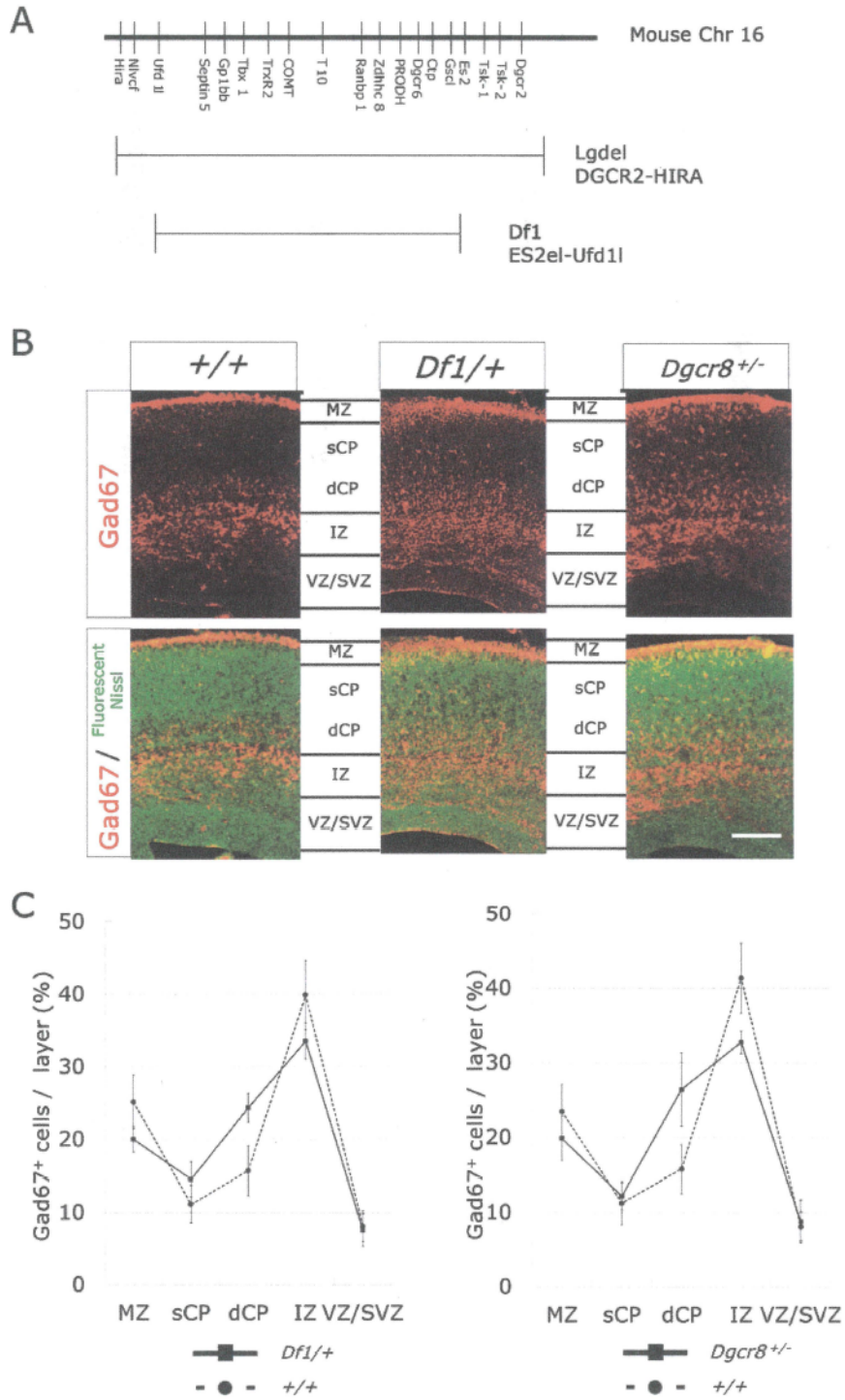
written consent for their participation.

Microarray analysis

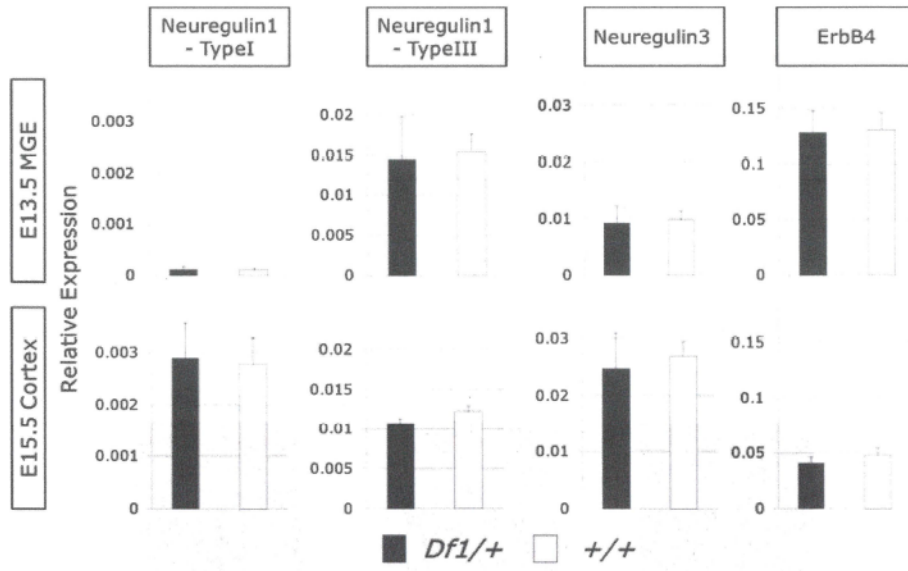
Total RNA from frontal cortex and striatum was extracted using the RNeasy Mini Kit (Qiagen) according to the manufacturer's instructions. The quality of RNA was 10 in RNA integrity number (RIN) score, which was assessed using a Bioanalyzer RNA 6000 Nano Chip (Agilent Technologies). Fragmented biotin-labeled cRNA were hybridized to Affymetrix U133Plus2.0 according to the manufacturer's protocols. Hybridization, washing, and scanning were conducted according to the manufacturer's instructions. Data analysis was performed using Partek Genomics Suite software (version 6.5). Raw intensities were normalized using *gcrma*. All microarray procedures were carried out at the Microarray Core Facility of Johns Hopkins University.

1. Wang Y, *et al.* (2012) CXCR4 and CXCR7 have distinct functions in regulating interneuron migration. *Neuron* 69(1):61-76.
2. Niwa H, Yamamura K, & Miyazaki J (1991) Efficient selection for high-expression transfectants with a novel eukaryotic vector. (Translated from eng) *Gene* 108(2):193-199 (in eng).
3. Kimoto S, *et al.* (2012) Selective overexpression of Comt in prefrontal cortex rescues schizophrenia-like phenotypes in a mouse model of 22q11 deletion syndrome. *Transl Psychiatry* 2:e146.
4. Ishizuka K, *et al.* (2010) Negative symptoms of schizophrenia correlate with impairment on the University of Pennsylvania smell identification test. *Neurosci Res* 66(1):106-110.

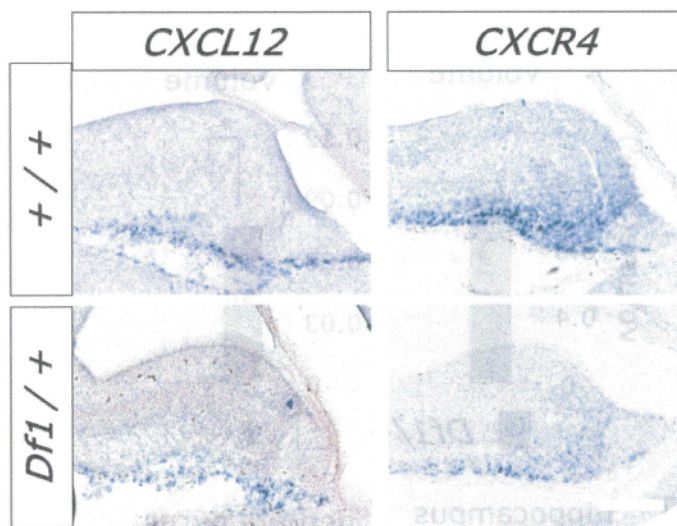
Supplementary Fig1



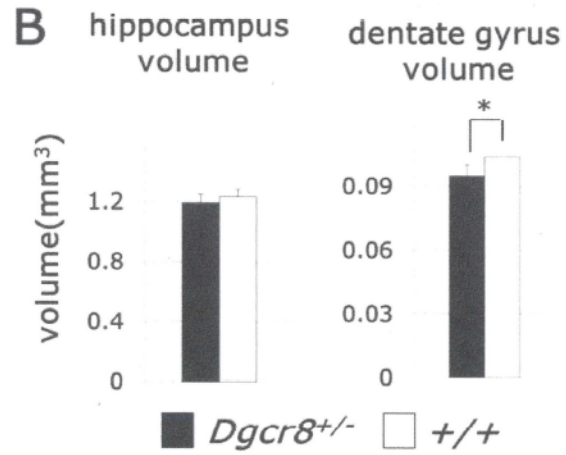
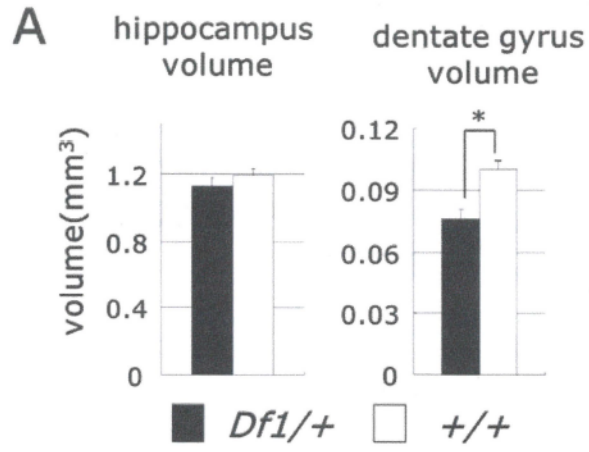
Supplementary-Fig2



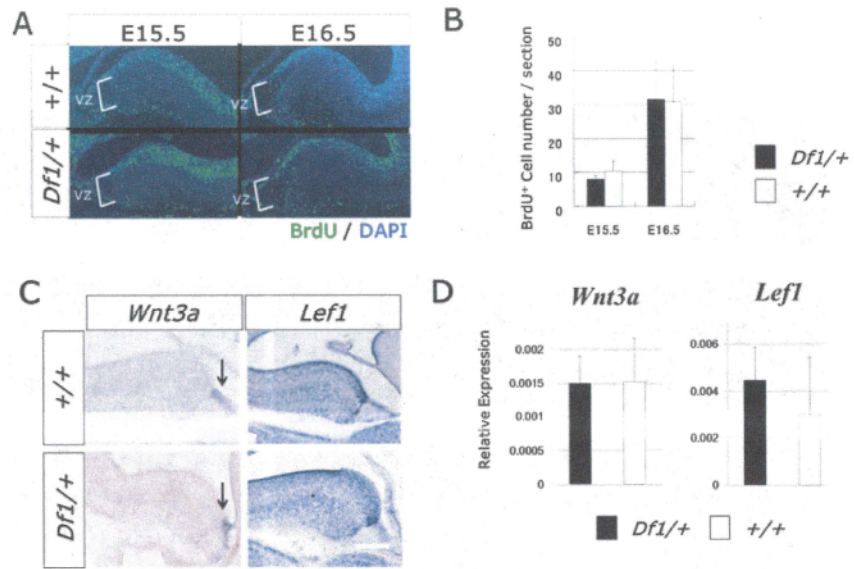
Supplementary-Fig3



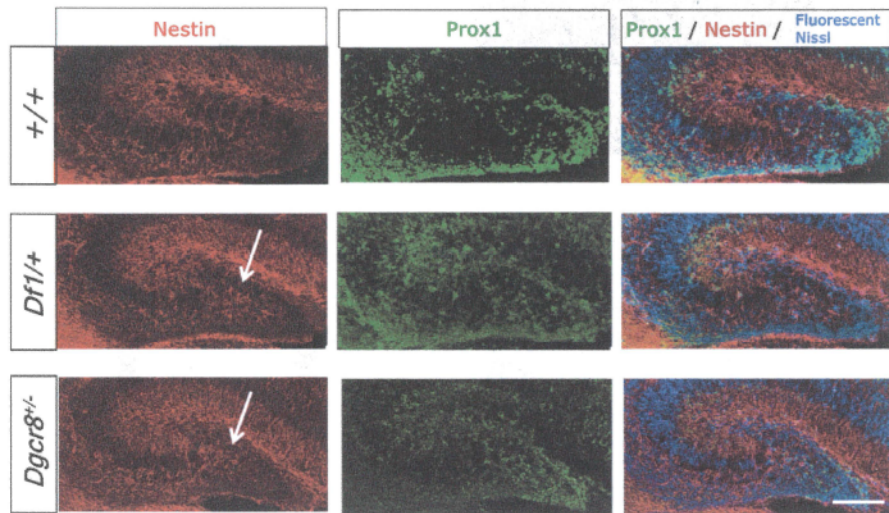
Supplementary-Fig4



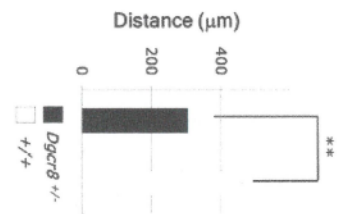
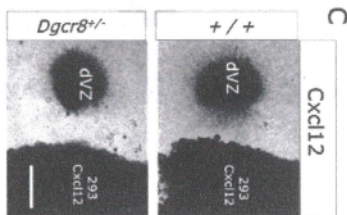
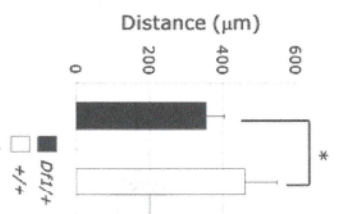
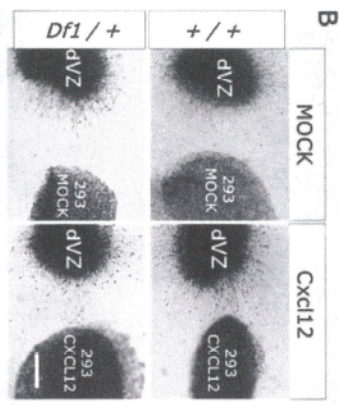
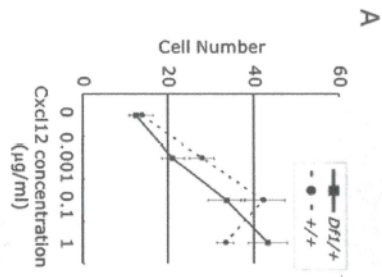
Supplementary-Fig5



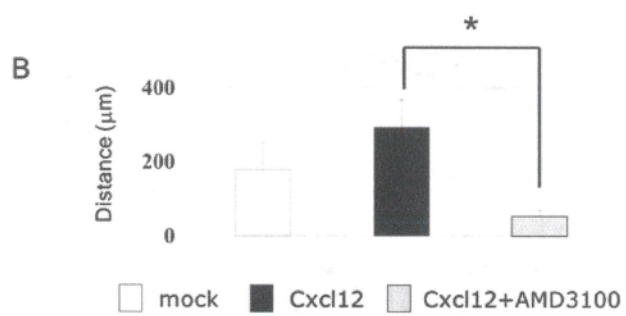
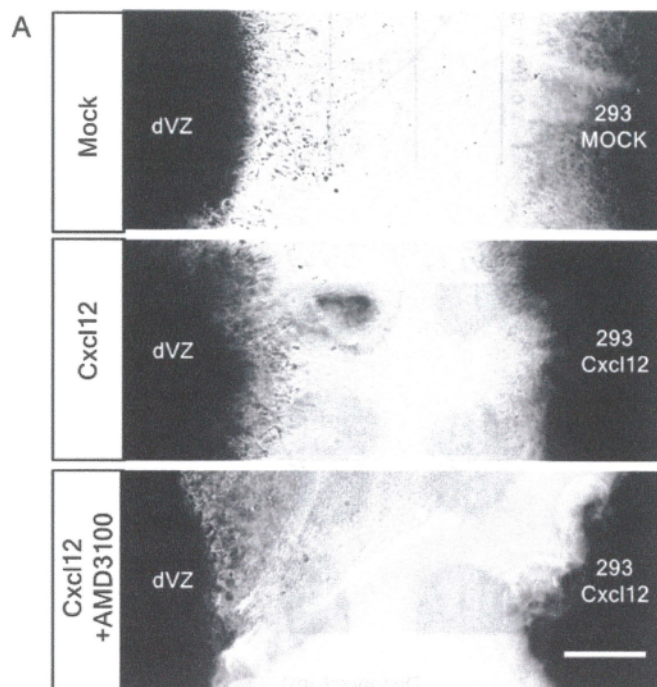
Supplementary-Fig6



Supplementary-Fig7



Supplementary-Fig8



Supplementary-Fig9

